J Mol Model (2010) 16:1931–1937
DOI 10.1007/s00894-010-0688-6

ORIGINAL PAPER

Theoretical studies on identity S_N2 reactions of lithium halide and methyl halide: A microhydration model

Shiyuan Zheng · Yan Xiong · Jinyue Wang

Received: 13 December 2009 / Accepted: 29 January 2010 / Published online: 20 March 2010

Abstract Reactions of lithium halide (LiX, X = F, Cl, Br and I) and methyl halide (CH_3X, X = F, Cl, Br and I) have been investigated at the B3LYP/6-31G(d) level of theory using the microhydration model. Beginning with hydrated lithium ion, four or two water molecules have been conveniently introduced to these aqueous-phase halogen-exchange S_N2 reactions. These water molecules coordinated with the center metal lithium ion, and also interacted with entering and leaving halogen anion *via* hydrogen bond in complexes and transition state, which to some extent compensated hydration of halogen anion. At 298 K the reaction profiles all involve central barriers ΔE_{cent} which are found to decrease in the order F > Cl > Br > I. The same trend is also found for the overall barriers (ΔE_{ovr}) of the title reaction. In the S_N2 reaction of sodium iodide and methyl iodide, the activation energy agrees well with the aqueous conductometric investigation.

Keywords B3LYP · Hydration · Lithium halide · Methyl halide · S_N2 reactions

S. Zheng · Y. Xiong (✉)
College of Chemistry and Chemical Engineering,
Chongqing University,
Chongqing 400044, China
email: xiong@cqu.edu.cn

J. Wang
Yibin Research Center of Chemical & Textile Industry,
Key Laboratory of Computational Physics in Universities of Sichuan,
School of Chemistry and Chemical Engineering, Yibin University,
Yibin 644000, China

S. Zheng
Department of Chemistry & Environment Science,
Chongqing University of Arts and Sciences,
Chongqing 402168, China

Introduction

Aqueous phase S_N2 reactions have been extensively studied by experimental method, since great attention was paid to gas-phase anion S_N2 reactions experimentally and theoretically [1–15]. Actual S_N2 reactions involve neutral reactants and some gas-phase ion pair reactions have been studied theoretically [16–20]. It is well known that the appearance of solvent can considerably change both the rate and order of homogeneous chemical reactions and solvent effect depends on charge types of S_N2 reactions. Several types of reactions affected by the solvent effect could be classified: (I) neutral molecule–anion reaction, (II) neutral molecule–neutral molecule reaction, (III) cation–anion reaction, and (IV) cation–neutral molecule reaction [21]. Furthermore, Westaway proposed a "solvation rule" for S_N2 reactions, that the solvent will not change the structure of the transition state for type I reactions, but will change it for type II reactions [22, 23]. Only type II, where the reactants are uncharged but the transition state has built up a charge, is aided significantly by polar solvents.

Reactions of lithium halide (LiX, X = F, Cl, Br and I) and methyl halide (CH_3X, X = F, Cl, Br and I) naturally belong to charge type II, where both lithium halide and methyl halide are neutral, and in transition states X is negatively charged. Necessarily, due to its strong polar and hydrogen bond donor, solvent water is very important for them. Along with this kind of reaction process, lithium halide in aqueous phase dissociates into free hydration structure of the lithium ion, *i.e.*, water-separated ion. Thereafter, hydrated lithium will interfere with halogen-exchanging reactions.

Recently, in view of involving neutral species throughout the reaction and the polarized continuum model (PCM) being less important there, an attractive treatment of microsolvation model was carried out with metal coordi-

nating solvent dimethyl ether to investigate the S_N2 reactions [24]. With introducing $Li(H_2O)_2^+$ and $Li(H_2O)_4^+$ to title reactions, we explore the hydration energies, potential energy surface of reactions and the role of hydrogen bond interaction in constructing complexes and transition states.

Methods

Computational details

The geometries of all the species were fully optimized using the hybrid density functional method B3LYP with 6-31G* basis sets [25–28]. All electron (AE) calculations were run for species containing F and Cl, and effective core potential (ECP) [29] for species containing Br and I. Charge distributions were calculated by the natural population analysis (NPA) at the B3LYP/6-31G* level [30–32]. In addition, the natural bond orbital (NBO) analysis was also carried out to observe the bond order change in the process of the reactions [9]. Reactants, products and complexes have zero imaginary frequencies and each transition state has only one imaginary frequency. The pathways between the transition structures and their corresponding minima have been identified by intrinsic reaction coordinate (IRC) calculation [33]. Throughout this paper, all inter-nuclear distances are in angstroms, all angles are in degrees, and relative energies are all in kJ mol^{-1} at 298 K. All calculations were performed using GAUSSIAN 03 system of programs [34].

Results and discussion

It is well-known that the nature of double-well potential curve comes to disappear when anion S_N2 reactions are carried out in protic solvents [1–3]. As mentioned in gas-phase anion S_N2 reactions [5–11], the energy profile for microhydrated nucleophilic substitution at carbon is described by a double-well potential curve (Fig. 1). The reaction involves the initial formation of a reactant dipole–dipole complex Comp[$n$$H_2O$], with a complexation energy ΔE_{comp}, relative to separated reactants $Li(H_2O)_nX$ and CH_3X (X = F, Cl, Br and I). This complex must overcome an activation barrier that we term the central barrier, ΔE_{cent}, to reach a C_2-symmetric transition structure TS[$n$$H_2O$], which then breaks down to give another product dipole–dipole complex Comp[$n$$H_2O$]. Finally, the product dipole–dipole complex dissociates into separated products $Li(H_2O)_nX$ and CH_3X. The overall barrier ΔE_{ovr} is designated to the gap between transition state TS[$n$$H_2O$] and separated reactants. For the set of identity reactions described here, reactants and products, reactant complexes and product complexes are of course identical. Total energies of the optimized species concerned for the title S_N2 reactions are listed in Table 1.

A. *$Li(H_2O)_n^+$ Structures*. Hydrated geometries of lithium ion with n=1~4 water molecules were calculated (Fig. 2). The interaction between water and lithium cation arises from the electrostatic attractability. The hydration $Li(H_2O)_n^+$ geometries with n=2, n=3 and n=4 correspond respectively to linear, trigonal and tetrahedral structures. An obvious character is that with the number of water increasing, the lengths of bond Li–O increase from 1.839 Å (n=1) to 1.949 Å (n=4) and the hydration energies also change from −180.3 kJ mol^{-1} (n=1) to −543.6 kJ mol^{-1} (n=4). The $Li(H_2O)_4^+$ provides the largest solvation energy and the tetrahedral coordination of Li^+ in water has also been suggested by some spectroscopic studies [35].
B. *$Li(H_2O)_nX$ and CH_3X (X = F, Cl, Br and I) Structures*. Calculated $Li(H_2O)_2X$ and $Li(H_2O)_4X$ geometries indicate that in the presence of X^-, the linear $Li(H_2O)_2^+$ structures are distorted with angles 132.6° (F), 159.7° (Cl), 155.2° (Br), 153.7° (I) and the tetrahedral structures of $Li(H_2O)_4^+$ are also broken (Fig. 3).

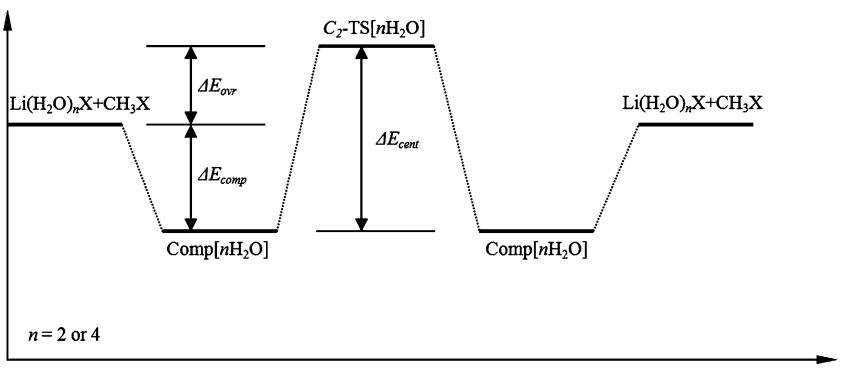

Fig. 1 Schematic energy profile for the identity exchange reactions Li(H2O)nX + CH3X (n=2 or 4; X = F, Cl, Br and I)

Table 1 Total energies (hartrees) for species and number of imaginary frequencies (*N*)

Species	*E* (298 K)	*N*	Species	*E* (298 K)	*N*
Li^+	−7.28313	0	Comp[$2H_2O$]	−1120.71511	0
$Li(H_2O)^+$	−83.73318	0	Comp[$4H_2O$]	−1273.54049	0
$Li(H_2O)_2^+$	−160.17439	0	TS[$2H_2O$]	−1120.66621	1
$Li(H_2O)_3^+$	−236.60281	0	TS[$4H_2O$]	−1273.49936	1
$Li(H_2O)_4^+$	−313.01917	0	X = Br		
H_2O	−76.38495	0	$Li(H_2O)_2Br$	−173.62060	0
TS[$2H_2O$](R) (X = F)	−399.89538	1	$Li(H_2O)_4Br$	−326.44844	0
TS[$4H_2O$]' (X = F)	−552.72494	1	CH_3Br	−53.04747	0
X = F			Comp[$2H_2O$]	−226.67602	0
$Li(H_2O)_2F$	−260.26095	0	Comp[$4H_2O$]	−379.50198	0
$Li(H_2O)_4F$	−413.09542	0	TS[$2H_2O$]	−379.46891	1
CH_3F	−139.69151	0	TS[$4H_2O$]	−226.63547	1
Comp[$2H_2O$]	−399.96877	0	X = I		
Comp[$4H_2O$]	−552.79785	0	$Li(H_2O)_2I$	−171.83377	0
TS[$2H_2O$]	−399.90029	1	$Li(H_2O)_4I$	−324.66118	0
TS[$4H_2O$]	−552.73366	1	CH_3I	−51.26307	0
X = Cl			Comp[$2H_2O$]	−223.10375	0
$Li(H_2O)_2Cl$	−620.63872	0	Comp[$4H_2O$]	−375.92995	0
$Li(H_2O)_4Cl$	−773.46685	0	TS[$2H_2O$]	−223.06883	1
CH_3Cl	−500.06739	0	TS[$4H_2O$]	−375.90141	1

Calculated CH_3X geometry parameters were listed in Table 2. It can be seen that they were in reasonable agreement with experimental ones. The theoretical C–X bond lengths differ from the experimental values by up to 0.037 Å (for CH_3Br) while the largest deviation for the C–H bond lengths is 0.007 Å (for CH_3Br). The calculated ∠XCH angles differ from experimental values by up to 0.9° (for CH_3I). We note that B3LYP calculation with 6-31G* basis sets gives a good agreement with experimental geometries for CH_3X systems.

Calculated charge distributions in the CH_3X molecules are presented in Table 3. These data show that fluorine atom in CH_3F bears considerable negative charge, contrasted with other CH_3X molecules where chlorine and bromine have almost zero charge while iodine a positive charge.

C. *Complexes*. The water around lithium cation binds with the halogen in CH_3X *via* hydrogen bond to form a series of complexes. The effects of $CH_3X\cdots Li(H_2O)_4X$ (X = F–I) complexation lie in 2-fold: (i) increasing the C–X bond distance in the free reactants CH_3X from 1.383 to 1.428 Å (X = F), 1.803 to 1.822 Å (X = Cl), 1.971 to 1.987 Å (X = Br) and 2.163 to 2.173 (X = I), respectively, and (ii) increasing the effective charge on the CH_3 group from +0.377 to +0.426 e for X = F, +0.082 to +0.129 e for X = Cl, +0.013 to +0.062 e for X = Br and −0.075 to −0.026 e for X = I, respectively. These two factors are favorable for the subsequent nucleophile attacking process. The Wiberg bond indices of C–X are 0.7911 for X = F, 0.9981 for Cl, 1.0105 for Br and 1.0129 for I with NBO analysis. The complexation energies ΔE_{comp} from X = F to I are found to decrease in the order 30.2 kJ mol^{-1} (F) > 17.3 kJ mol^{-1} (Cl) > 16.8 kJ mol^{-1} (Br) > 15.8 kJ mol^{-1} (I) (Table 4) and show a very good linear correlation with their electronegativities of X using the Pauling (R^2=0.922), Mulliken (R^2=0.898) (Fig. 4) or Allred-Rochow (R^2=0.933) scales [40].

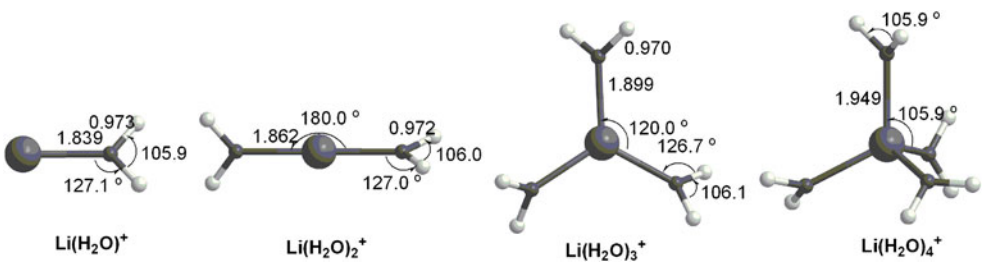

Fig. 2 Hydration geometries of lithium ion with *n*=1~4 water molecules

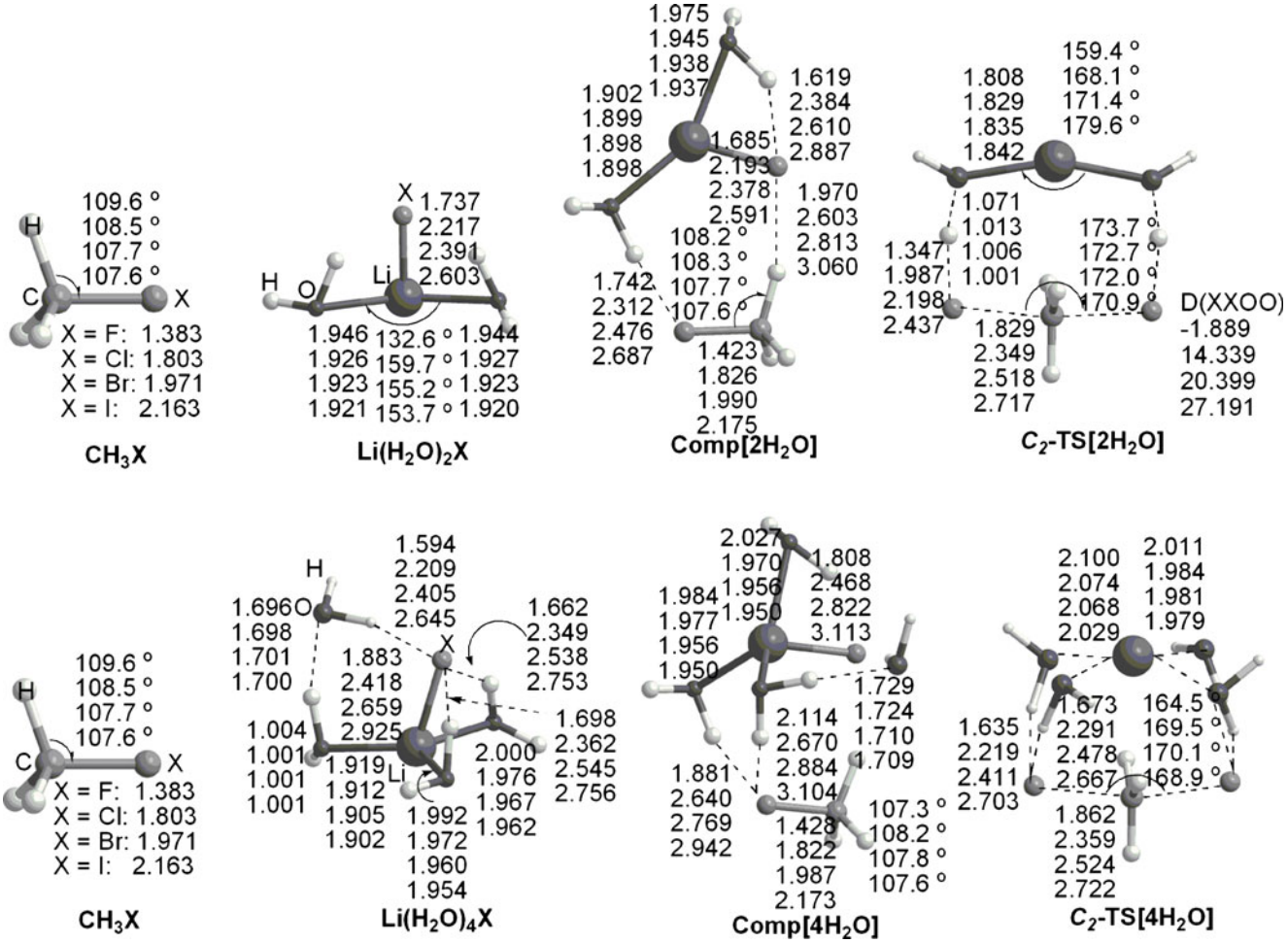

Fig. 3 Geometries of methyl halide, complexes and transition states

In $CH_3X\cdots Li(H_2O)_2X$ (X = F-I) complexes, C–X bonds are elongated with one hydrogen of water binding halogen atom. Compared with $CH_3X\cdots Li(H_2O)_4X$ complexes, $CH_3X\cdots Li(H_2O)_2X$ complexes indicate higher complexation energies 45.2 kJ mol^{-1} (X = F), 24.9 kJ mol^{-1} (X = Cl), 22.0 kJ mol^{-1} (X = Br) and 19.1 kJ mol^{-1} (X = I), resulted from shorter H-bonds 1.742 Å (X = F), 2.312 Å (X = Cl), 2.476 Å (X = Br) and 2.687 Å (X = I). Complexation energies are found to correlate well with H-bond lengths (R^2=0.964) (Fig. 5) as well as Mulliken electronegativity of X (R^2=0.955) (Fig. 4).

Table 2 Calculated and experimental geometries of CH_3X (X = F, Cl, Br and I)

Species	Level	*r*(C–X)	*r*(C–H)	∠XCH	*μ*(dye)
CH_3F	B3LYP/6-31G(d)	1.383	1.097	109.6	1.714
	B3LYP/6-31G+(d,p)[a]	1.396	1.092	108.6	2.085
	expt[b]	1.383	1.086	108.8	1.858
CH_3Cl	B3LYP/6-31G(d)	1.803	1.090	108.5	2.084
	B3LYP/6-31G+(d,p)[a]	1.806	1.087	108.3	2.106
	expt[c]	1.776	1.085	108.6	1.892
CH_3Br	B3LYP/6-31G(d)-ECP	1.971	1.089	107.8	2.075
	B3LYP/6-31G+(d,p)-ECP[a]	1.969	1.086	107.7	2.026
	expt[d]	1.934	1.082	107.7	1.822
CH_3I	B3LYP/6-31G(d)-ECP	2.163	1.088	107.7	1.853
	B3LYP/6-31G+(d,p)-ECP[a]	2.159	1.085	107.6	1.793
	expt[e]	2.132	1.085	108.6	1.620

[a] From Ref [18]
[b] From Ref [36]
[c] From Ref [37]
[d] From Ref [38]
[e] From Ref [39]

Table 3 NPA charge distributions for CH_3X (X = F, Cl, Br and I)

Species	q(X)	q(C)	q(H)
CH_3F	−0.377	−0.183	0.186
CH_3Cl	−0.082	−0.650	0.244
CH_3Br	−0.013	−0.752	0.255
CH_3I	0.075	−0.851	0.258

D. *Transition states.* Geometries of transition states, TS $[2H_2O](I)$ (X = F) (Fig. 3) and TS$[2H_2O](R)$ (X = F) (Fig. 6), with two water molecules represent respectively inversion (I) and retention (R) approaches of the reaction of $Li(H_2O)_2F$ and CH_3F, and imaginary frequencies 542.28i cm^{-1} and 616.49i cm^{-1} respectively associate with their C–F stretching vibration models. The former shows lower energies than the latter by 15.4 kJ mol^{-1}. Its conclusion is rationally reverse to the gas ion pair S_N2 reaction [18]. The presence of hydrogen bonding makes inversion structure a larger angle of F-C-F than retention one, and weakens electrostatic repulsion between $F^{\delta-}$ and $F^{\delta-}$ to produce lower energy. Contrasted with TS$[4H_2O]$ (X = F) (Fig. 3), TS$[4H_2O]$' (X = F) (Fig. 6) lies two H-bonds with F atoms. Four hydrogen bonds can reduce the energy by 24 kJ mol^{-1}. So, 4-hydrogen bond TS with inversion configuration is favorable for this series of S_N2 reactions.

In C_2-symmetric transition states TS$[4H_2O]$, compared with its complexes, the Wiberg bond indices of C–X decrease and are 0.3992 for X = F, 0.4621 for X = Cl, 0.4775 for X = Br and 0.4889 for X = I, respectively. An obvious geometrical feature is that angles X-C-X slightly twist, different from linear structure in anionic S_N2 reactions X^- + CH_3X, and decrease in the range of 9.9~15.5°, resulted from 4-hydrogen bond bridging. Li^+ cation is surrounded by water molecules, which are almost in a plane structure furthest to form 4 hydrogen bonds. The deformation of X-C-X would be responsible for the higher central barrier than the gas-phase anion S_N2 reaction [5–11].

Table 4 Complexation energies (ΔE_{comp}), central barriers (ΔE_{cent}) and overall barriers (ΔE_{ovr}) of reactions $Li(H_2O)_nX + CH_3X$ (n=2 or 4, X = F, Cl, Br and I)

Species	ΔE_{comp}		ΔE_{cent}		ΔE_{ovr}	
	n=2	n=4	n=2	n=4	n=2	n=4
X = F	−45.2	−30.2	189.7	177.8	144.5	147.5
X = Cl	−24.9	−17.3	135.4	113.9	110.5	96.6
X = Br	−22.0	−16.8	112.3	91.6	90.3	74.8
X = I	−19.1	−15.8	96.7	79.1	77.6	63.3

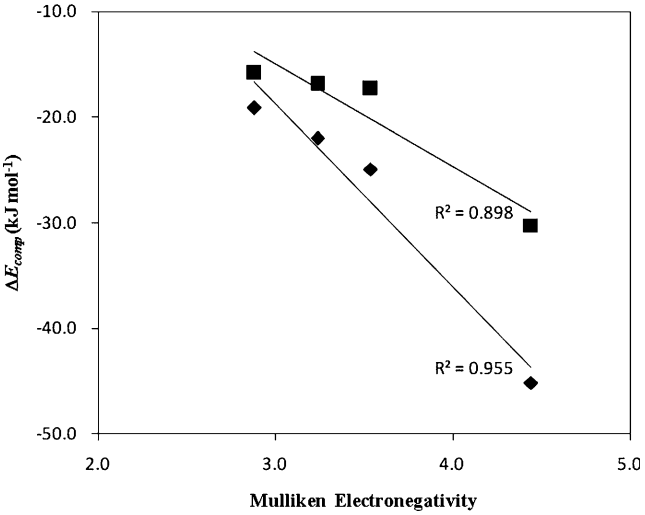

Fig. 4 Plots of complexation energies vs Mulliken electronegativity of X (X = F, Cl, Br and I). Symbol ■ represents the reactions $Li(H_2O)_4X$ + CH_3X, Symbol ♦ represents the reactions $Li(H_2O)_2X$ + CH_3X. Definition of Mulliken electronegativity is $\chi_M = (I + A)/2$, where I and A are experimental ground state first ionization potentials and electron affinities, respectively. Pauling units (χ_M values from [40])

Another distinct change is the elongation of bond C–X of TSs relative to CH_3X moieties of complexes and the percent of elongation $\%C–X^{\neq}$ is 30.3 for X = F, 29.5 for Cl, 27.0 for Br and 25.3 for I, respectively.

The central activation barriers ΔE_{cent} in the reactions are all positive, varying from 79.1 kJ mol^{-1} for X = I up to 177.8 kJ mol^{-1} for X = F (Table 4). Some factors that might influence the barrier heights have been discussed. A very

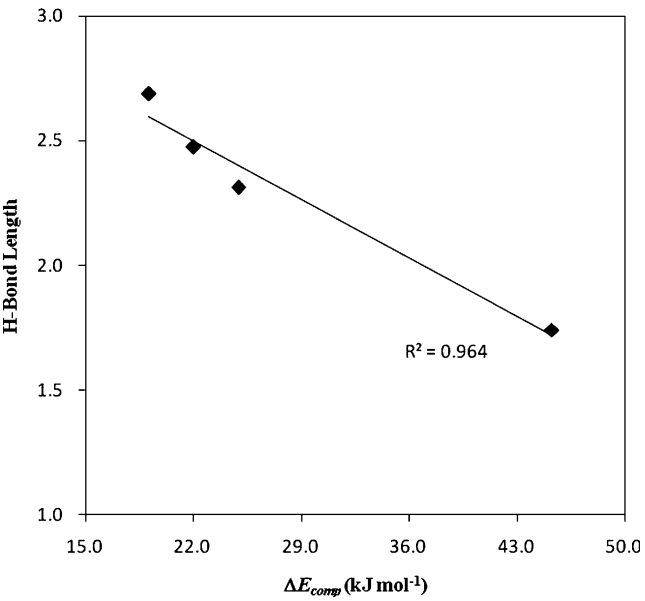

Fig. 5 Plot of complexation energies vs the lengths of hydrogen bond HOH···XCH_3 (X = F, Cl, Br and I) in the Comp$[2H_2O]$

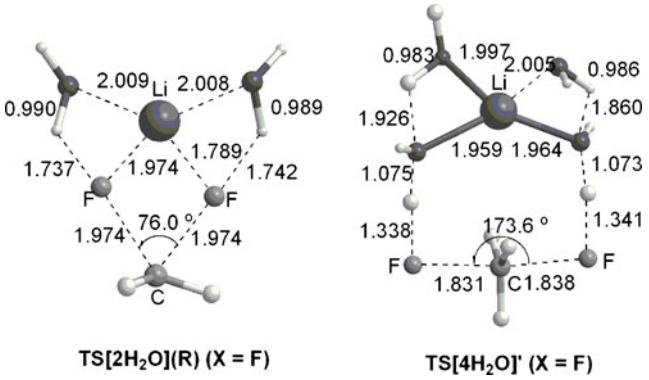

Fig. 6 Geometries of retention TS[$2H_2O$] (X = F) and TS[$4H_2O$]' (X = F)

good linear relationship between the central barriers and the experimentally available bond dissociation energies $D_{C–X}$ is found (R^2=0.986) [41]. The Mulliken electronegativity of X has a good linear relationship with central activation barrier ΔE_{cent} (R^2=0.988) (Fig. 7). The percent of elongation %C–$X^{\neq}$ shows a correlation of R^2=0.756 with the central barrier. Since it may be an artifact of the RRKM model and the Marcus analysis, a linear correlation between the experimental central barriers and the methyl cation affinities (MCAs) of X^-has been previously noted [42]. We find a linear correlation between our calculated central barriers and the experimental MCAs of X^-(R^2=0.993) (Fig. 8) [41]. The overall barriers ΔE_{ovr} are also found to correlate well with experimental MCAs of X^-(R^2=0.993).

In C_2-symmetric transition states TS[$2H_2O$], the angles X-C-X vary from 170.9 for X = I to 173.7 for X = F. Only two H-bonds in TS[$2H_2O$] are responsible for the higher central barrier than that in the TS[$4H_2O$]. The central activation barriers ΔE_{cent} are all positive, varying from

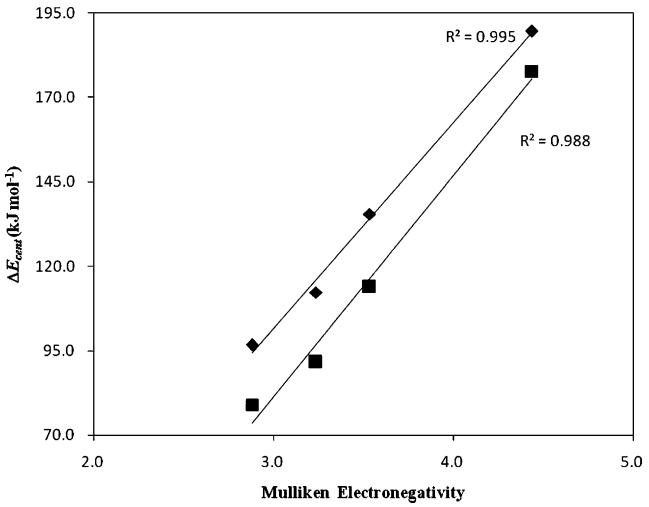

Fig. 7 Plots of central barriers vs Mulliken electronegativity of X (X = F, Cl, Br and I). Symbol ■ represents the reactions Li$(H_2O)_4$X + CH_3X, Symbol ♦ represents the reactions Li$(H_2O)_2$X + CH_3X

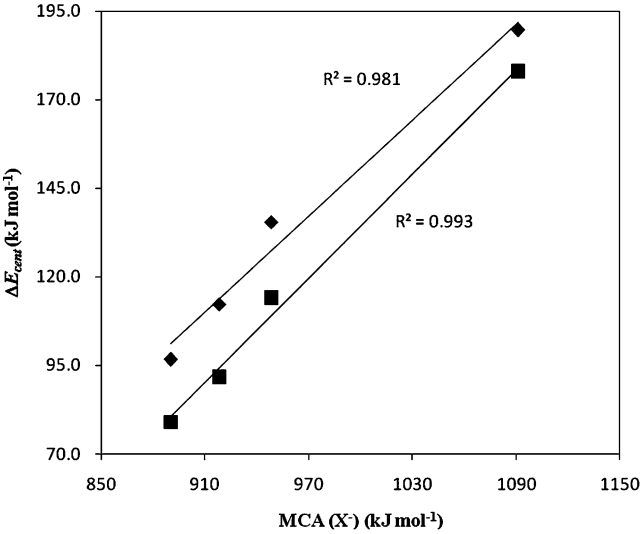

Fig. 8 Plots of central barriers vs methyl cation affinities (MCAs) of X (X = F, Cl, Br and I). Symbol ■ represents the reactions Li$(H_2O)_4$X + CH_3X, Symbol ♦ represents the reactions Li$(H_2O)_2$X + CH_3X

96.7 kJ mol^{-1} for X = I up to 189.7 kJ mol^{-1} for X = F, and is also found to be in very good linear relationships with the experimentally available bond dissociation energies $D_{C–X}$ (R^2=0.997), the experimental MCAs of X^- (R^2=0.981) (Fig. 8) and the Mulliken electronegativity of X (R^2=0.995) (Fig. 7). The overall barriers ΔE_{ovr} also have good linear relationships with experimental $D_{C–X}$ (R^2=0.996) and MCAs of X^- (R^2=0.953).

In reactions Na$(H_2O)_4$X + CH_3X, the decreasing activation energies and Gibbs free energy and increasing reaction rate from X = F to X = I are demonstrated in Table 5. Compared with the structure of TS[$4H_2O$] (X = I) (Fig. 3), substitution of sodium ion with bigger ion radius obtains larger angle (X-C-X) of 172.4° and shorter C···X distance of 2.718 Å. In the reaction of sodium iodide and methyl iodide, the activation energies and Gibbs free energy both reduce, larger reaction rate is attained, and reaction activation energy (77.2 kJ mol^{-1}) is found to be very close to the experimental result (77.6±0.9 kJ mol^{-1}) in aqueous-phase reaction [1], which suggests the rationality of our proposed pseudo-aqueous model.

Table 5 Relative parameters for series of reactions

X	ΔE_{cent} (298K)	%C-$X^{\neq}$	ΔG_{cent} (298K)	Lnk
F	177.5	30.3	192.4	−19.2
Cl	112.9	29.5	127.7	−8.4
Br	91.6	27.0	104.3	−4.5
I	79.1	25.3	92.6	−2.6
I[a]	77.2 (77.6±0.9)	25.1	79.7	−0.5

[a] Treatment of sodium iodide and methyl iodide. Value of experimental activation energy in bracket

Summary and conclusions

DFT calculations were carried out on the reactions of lithium halide (LiX, X = F, Cl, Br and I) and methyl halide (CH_3X, X = F, Cl, Br and I). The stationary geometries of various involved species were fully optimized at the B3LYP/6-31G(d) level of theory. At 298 K the reaction profiles introducing $Li(H_2O)_4^+$ all involve central barriers ΔE_{cent} which decrease in the order F (177.8 kJ mol^{-1}) > Cl (113.9 kJ mol^{-1}) > Br (91.6 kJ mol^{-1}) > I (79.1 kJ mol^{-1}). The overall barriers relative to the reactants (ΔE_{ovr}) are 147.5 kJ mol^{-1} (X = F), 96.6 kJ mol^{-1} (X = Cl), 74.8 kJ mol^{-1} (X = Br), 63.3 kJ mol^{-1} (X = I), respectively. The stabilization of the complexes decreases in the following order, F (30.2 kJ mol^{-1}) > Cl (17.3 kJ mol^{-1}) > Br (16.8 kJ mol^{-1}) > I (15.8 kJ mol^{-1}) and shows a very good linear correlation with electronegativity of X using Pauling (R^2=0.922), Mulliken (R^2=0.898) or Allred-Rochow (R^2=0.933) scale. Activation energies decreasing from X = F to I linearly correlate with the experimental MCAs of X^-(R^2=0.993). Introduction of linear $Li(H_2O)_2^+$ leads to similar results. Furthermore, compared with conductometric result (77.6±0.9 kJ mol^{-1}) of activation energy in aqueous-phase reaction, reaction between NaI and CH_3I was examined and provided close activation energy of 77.2 kJ mol^{-1}. Next work is still under way to design and further understand the solution-phase S_N2 reaction.

Acknowledgments We thank Scientific Research Funding of Chongqing University, Innovative Talent Training Project of Chongqing University, the Third Stage of "211 project" (No. S-09103), Chongqing Municipal Education Commission (No. KJ-091201) and Bureau of Education of Sichuan Province (No. 2006ZD051) for financial support.

References

1. For experimental investigation on aqueous-phase S_N2 reactions, see a review: Parker AJ (1969) Chem Rev 69:1–32 and its cited references
2. Dewar MJS, Dougherty RC (1975) The PMO theory of organic chemistry. Plenum, New York, p 234
3. Arnett EM, Johnston DE, Small LE (1975) J Am Chem Soc 97:5598–5600
4. Olmstead WN, Brauman JI (1977) J Am Chem Soc 99:4219–4228
5. DePuy CH, Gronert S, Mullin A, Bierbaum VM (1990) J Am Chem Soc 112:8650–8655
6. Pellerite MJ, Brauman JI (1983) J Am Chem Soc 105:2672–2680
7. Caldwell G, Magnera TF, Kebarle P (1984) J Am Chem Soc 106:959–966
8. Shi Z, Boyd RJ (1990) J Am Chem Soc 112:6789–6796
9. Glukhovtsev MN, Pross A, Radom L (1995) J Am Chem Soc 117:2024–2032
10. Glukhovtsev MN, Bach RD, Pross A, Radom L (1996) Chem Phys Lett 260:558–564
11. Glukhovtsev MN, Pross A, Schlegel HB, Bach RD, Radom L (1996) J Am Chem Soc 118:11258–11264
12. Glad SS, Jensen F (1997) J Am Chem Soc 199:227–232
13. Cossi M, Adamo C, Barone V (1998) Chem Phys Lett 297:1–7
14. Safi B, Choho K, Geerlings P (2001) J Phys Chem A 105:591–601
15. Kato S, Davico GE, Lee HS, DePuy CH (2001) Int J Mass Spectrom 210–211:223–229
16. Harder S, Streitwieser A, Petty JT, Schleyer PvR (1995) J Am Chem Soc 117:3253–3259
17. Streitwieser A, Choy GSC, Abu-Hasanayn F (1997) J Am Chem Soc 119:5013–5019
18. Xiong Y, Zhu HJ, Ren Y (2003) J Mol Struct THEOCHEM 664–665:279–289
19. Ren Y, Chu SY (2004) J Comput Chem 25:461–467
20. Hasanayn F, Streitwieser A, Al-Rifai R (2005) J Am Chem Soc 127:2249–2255
21. Ingold CK (1969) Structure and mechanism in organic chemistry. Cornell University Press, Ithaca, p 457
22. Westaway KC (1978) Can J Chem 56:2691–2699
23. Westaway KC, Lai ZG (1989) Can J Chem 67:345–349
24. Streitwieser A, Jayasree EG (2007) J Org Chem 72:1785–1798
25. Lee C, Yang W, Parr RG (1988) Phys Rev B 37:785–789
26. Becke AD (1988) Phys Rev A 38:3098–3100
27. Miehlich B, Savin A, Stoll H, Preuss H (1989) Chem Phys Lett 157:200–206
28. Becke AD (1993) J Chem Phys 98:5648–5652
29. Wadt WR, Hay PJ (1985) J Chem Phys 82:284–298
30. Reed AE, Weinstock RB, Weinhold F (1985) J Chem Phys 83:735–746
31. Foster JP, Weinhold F (1980) J Am Chem Soc 102:7211–7218
32. Reed AE, Curtiss LA, Weinhold F (1988) Chem Rev 88:899–926
33. Gonzalez C, Schlegel HB (1990) J Phys Chem 94:5523–5527
34. Frisch MJ, Trucks GW, Schlegel HB et al (2004) Gaussian 03, Revision E.01. Gaussian, Wallingford
35. Michaellian KH, Moskovits M (1978) Nature 273:135–136
36. Egawa T, Yamamoto S, Nakata M, Kuchitsu K (1987) J Mol Struct 156:213–228
37. Jensen T, Brodersen S, Guelachvili G (1981) J Mol Spectrosc 88:378–393
38. Graner G (1981) J Mol Spectrosc 90:394–438
39. Harmony MD, Laurie VW, Kuczkowski RL, Ramsay DA, Lovas FJ, Lafferty WJ, Maki AG (1979) J Phys Chem Ref Data 8:619–711
40. For the data, see: Allen LC (1989) J Am Chem Soc 111:9003–9014
41. Lias SG, Bartmess JE, Liebman JF, Holmes JL, Levin RD, Mallard WG (1988) J Phys Chem Ref Data 17 Suppl. 1
42. Han CC, Dodd JA, Brauman JI (1986) J Phys Chem 90:471–477